Article

Declining precipitation frequency may drive earlier leaf senescence by intensifying drought stress and enhancing drought acclimation

Xinyi Zhang[1,2,3], Xiaoyue Wang [1,2] ✉, Constantin M. Zohner [4], Josep Peñuelas [5,6], Yang Li [7], Xiuchen Wu [8], Yao Zhang [9], Huiying Liu [10], Pengju Shen [1,2], Xiaoxu Jia[1,2], Wenbin Liu [1,2], Dashuan Tian [2,6], Prajal Pradhan [11,12], Adandé Belarmain Fandohan [13], Dailiang Peng [14] ✉ & Chaoyang Wu [1,2] ✉

Precipitation is an important factor influencing the date of foliar senescence, which in turn affects carbon uptake of terrestrial ecosystems. However, the temporal patterns of precipitation frequency and its impact on foliar senescence date remain largely unknown. Using both long-term carbon flux data and satellite observations across the Northern Hemisphere, we show that, after excluding impacts from of temperature, radiation and total precipitation by partial correlation analysis, declining precipitation frequency may drive earlier foliar senescence date from 1982 to 2022. A decrease in precipitation frequency intensifies drought stress by reducing root-zone soil moisture and increasing atmospheric dryness, and limit the photosynthesis necessary for sustained growth. The enhanced drought acclimation, showing a more rapid response to drought, also explains the positive relationship between precipitation frequency and foliar senescence date. Finally, we find 30 current state-of-art Earth system models largely fail to capture the sensitivity of DFS to changes in precipitation frequency and incorrectly predict the direction of correlations for approximately half of the northern global lands, in both historical simulations and future predictions. Our results therefore highlight the critical need to include precipitation frequency, rather than just total precipitation, into models to accurately forecast plant phenology under future climate change.

Plant phenology is greatly affected by ongoing changing climate[1–3]. While spring leaf-out is typically driven by temperature, where warming leads to earlier spring leaf-out[4], predicting temporal changes in the dates of autumn foliar senescence (DFS) is more complex due to the multitude of influencing factors. Across northern terrestrial ecosystems, observations and model predictions of DFS are mixed, with both earlier and later senescence reported under different conditions[5,6]. For example, rising temperatures late in the season can delay DFS given sufficient water availability[7]. Conversely, warmer conditions can also speed up seasonal development, resulting in

earlier DFS[8]. Moreover, water availability plays a crucial role in autumn phenology, with severe droughts causing earlier DFS[9]. Thus, understanding the impact of water availability on DFS changes is becoming increasingly vital in the context of climate change[10], especially with the expectation of more frequent and severe droughts in the future[11,12].

Precipitation is essential for plant growth, particularly through the replenishment of soil moisture[13]. However, its impact on DFS varies widely, with both positive and negative effects reported. This inconsistency is likely due to local environmental factors, such as the amount of annual precipitation, and geophysical conditions like topography[14]. The complexity of these patterns and the lack of a clear understanding of the underlying processes make it challenging to accurately model the effects of precipitation on DFS. Previous researches have primarily focused on the total amount of precipitation, but recent studies suggest that it is also essential to consider the temporal patterns of precipitation, such as frequency and intensity, which may have a more pronounced impact on plant phenology[15–17]. For instance, changes in the frequency of rainfall events, especially prolonged dry periods between events, have been shown to shorten the growth period of various plant species[18]. In arid and semi-arid ecosystems, shifts in rainfall frequency have been found to significantly alter plant physiological response, such as water uptake efficiency and photosynthesis rates, which could ultimately affect DFS[19]. A previous study found that leaf onset date is impacted more by precipitation frequency than by its total amount[16]. This finding is also crucial for understanding DFS, as vegetation tends to be more sensitive to water availability in autumn than in spring[20], which would affect ecosystem carbon balance, productivity, and climate feedbacks differently than leaf onset. Therefore, the focus should not be limited to the total precipitation amount but should also encompass its temporal distribution, such as frequency, to better understand its effects on DFS.

Northern hemisphere includes a diverse range of climate zones, vegetation types, and precipitation regimes, making it an ideal region to examine how different precipitation patterns affect DFS. Furthermore, the Northern Hemisphere contains most of the world's terrestrial vegetation, and phenological changes here significantly impact global biogeochemical cycles and climate systems[21]. In addition, different plant functional types may respond in diverse ways to changes in precipitation patterns due to their varying physiological traits and adaptations[22]. Therefore, we aimed to explore the responses and the underlying reasons of DFS to changes in precipitation frequency across the Northern Hemisphere.

In this work, we used DFS derived from long-term flux measurements and satellite observations (Supplementary Fig. 1, Supplementary Data 1–2), combined with precipitation frequency data from gridded meteorological datasets (both ERA5 and CRU) (Supplementary Fig. 2). Additionally, we evaluated the capability of current state-of-the-art Earth system models to reproduce the observed relationships between DFS and precipitation frequency (Supplementary Fig. 3, Supplementary Data 3–4). We show that declining precipitation frequency (P_{freq}) is associated with earlier DFS from 1982 to 2022. Reduced P_{freq} may exacerbate drought stress and potentially enhance the drought acclimation of plants. Moreover, 30 current state-of-the-art Earth system models fail to accurately represent the sensitivity of DFS to changes in P_{freq}, with nearly half of the northern global land area showing incorrect correlation directions in both historical simulations and future projections across various shared socioeconomic pathways.

Results

We observed a widespread decline in P_{freq} across the Northern Hemisphere between 1982 and 2022 from both the ERA5 and CRU data (Supplementary Fig. 4). By controlling preseason temperature and radiation through partial correlation analysis, we observed negative correlations between DFS and total precipitation at higher latitudes

(>50 degrees), whereas positive correlations between DFS and precipitation were more common at lower latitudes (Fig. 1A). Overall, the proportions of significantly negative and positive DFS-precipitation correlations were 15.6% and 9.5%, respectively. These proportions slightly changed to 17.4% vs. 8.8% when accounting for the effects of precipitation frequency using partial correlation (Fig. 1B). In comparison, P_{freq} was mostly positively correlated with DFS, with 57.7% of correlations being positive and 14.9% being significantly positive, about double the proportion of significant negative correlations (7.8%) (Fig. 1C). Further analysis, illustrated in a Sankey diagram, showed that considering the impact of P_{freq} significantly reduced the strength of negative DFS-precipitation relationships (Supplementary Fig. 5). This trend remained consistent across different plant functional types (Fig. 1D–F). We also plotted the distributions of the total precipitation-DFS and P_{freq}-DFS correlations in the total precipitation and frequency space (Supplementary Fig. 6). We found earlier DFS with increased total precipitation often occurred when precipitation frequency exceeded an empirical threshold of 15. In comparison, the positive correlations between precipitation frequency and DFS were overall broadly consistent, and earlier DFS with increased frequency was observed only for low precipitation frequency but with extreme total precipitation. Flux measurements showed similar patterns (Fig. 1G–I): The correlation between P_{freq} and DFS was predominantly positive (23.1% positive vs. 5.7% negative), whereas the correlation between total precipitation and DFS was equally positive and negative (15.8% positive vs. 15.3% negative).

We used a structural equation model (SEM) to explore the underlying mechanisms that may explain the predominantly positive correlation between P_{freq} and DFS (Fig. 2A). We found that both total precipitation and P_{freq} significantly decreased radiation (path effect of −0.42, −0.43, respectively). In comparison, while both P_{freq} and total precipitation positively impacted root zone soil moisture, the influence of P_{freq} was stronger (path coefficients of 0.50, $P < 0.01$, and 0.44, $P < 0.01$, respectively). In particular, atmospheric dryness, represented by vapor pressure deficit, increased significantly with declined P_{freq} than with total precipitation, with path effects of −0.51 ($P < 0.01$) and −0.35 ($P < 0.05$), respectively. This suggests that declines in precipitation frequency have a more severe impact on plant drought stress than changes in total precipitation, which in turn causes earlier leaf senescence in many regions.

We also found a significantly positive relationship between P_{freq} and the drought response lag ($R^2 = 0.40$, $p < 0.05$), indicating that plants acclimate to drought more quickly with decreased P_{freq}, necessitating longer recovery times from drought ($R^2 = 0.82$, $p < 0.05$, Fig. 2B, C). Using a moving window approach, we observed an increasing importance of P_{freq} in regulating DFS changes over the past four decades, indicated by increases in the slope values (Fig. 2D). We further found that decreased P_{freq} was often associated with a smaller size of a single rain event (11.7% and 0.9% for positive and negative correlations, respectively), reducing soil moisture accumulation (Fig. 2E) and thereby contributing to the increased soil moisture variability and earlier DFS consequently ($R^2 = 0.64$, $P < 0.01$, Fig. 2F).

We further tested if the positive impacts of P_{freq} on DFS could be reproduced by current state-of-the-art Earth system models. This included both Trendy models for historical simulations and CMIP6 models for future projections under various shared socioeconomic pathways (SSPs), including SSP126, SSP245, SSP370, and SSP585. We found that Trendy models overall captured the relationship between DFS and precipitation frequency, with larger proportions of significant positive correlations (Fig. 3A). Similarly, among the 14 CMIP6 models, only three failed to reproduce the observed patterns (ACCESS-ESM1-5, BCC-CSM2-MR and TaiESM1). However, when assessing the sensitivity of DFS to changes in P_{freq} (i.e., how DFS changes per unit variation in P_{freq}), we observed substantial differences among models (Fig. 3B). Only seven out of 16 Trendy models demonstrated positive
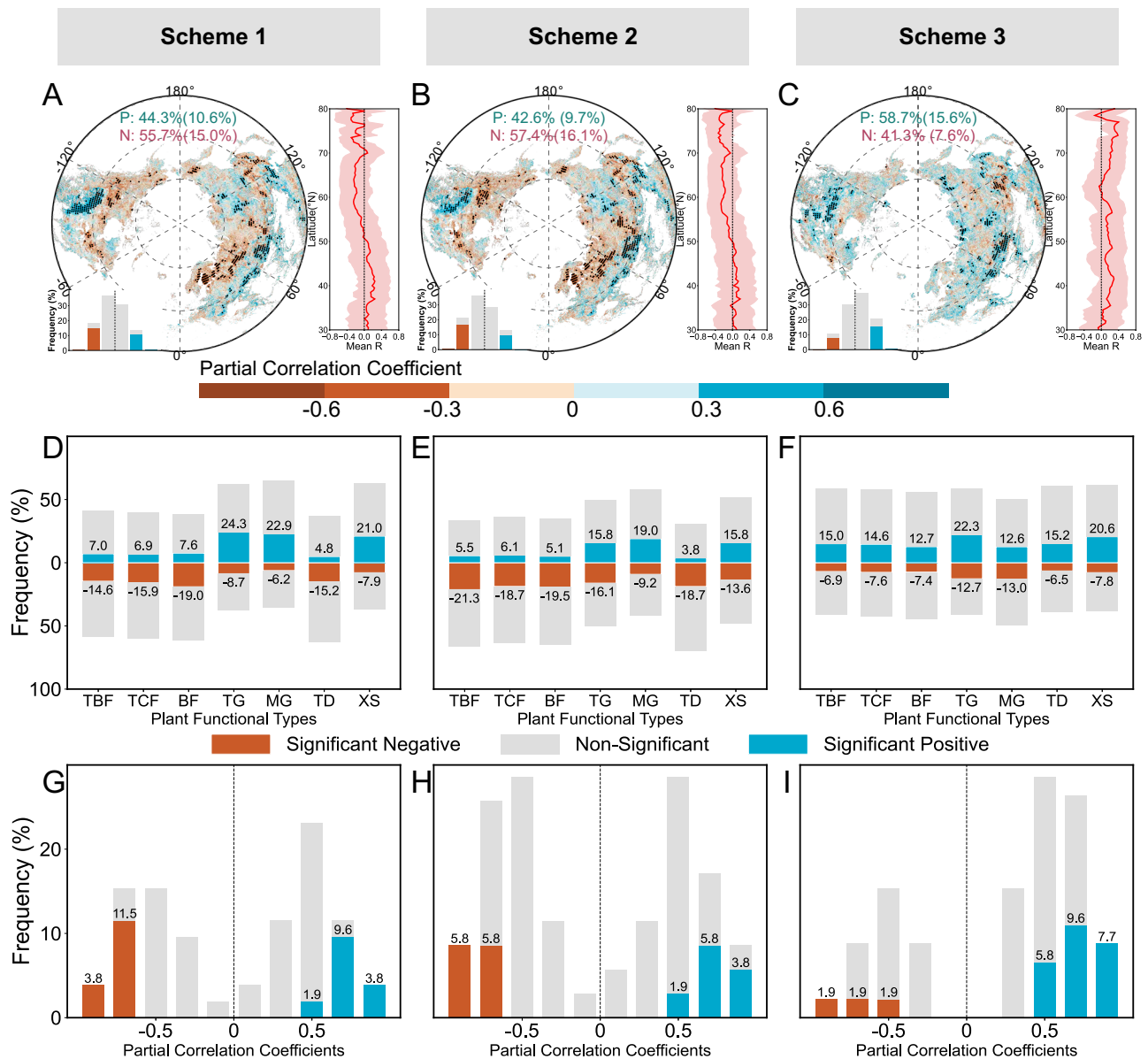
Fig. 1 | Relationships between the dates of leaf senescence (DFS) and precipitation changes. Scheme 1 (**A**, **D**, **G**) conducts partial correlations analysis between DFS and total precipitation, controlling only temperature and radiation, and Scheme 2 (**B**, **E**, **H**) by additionally controlling precipitation frequency. Scheme 3 (**C**, **F**, **I**) is partial correlations between DFS and precipitation frequency, controlling temperature, radiation and total precipitation. **A**–**C** Represent the results from satellite observations. Panels (**D**–**F**) are the results classified by plant functional type, including temperate broadleaf forests (TBF), temperate coniferous forests (TCF), boreal forests (BF), temperature grasslands (TG), montane grasslands (MG), tundra (TD), and xeric shrublands (XS). Panels (**G**–**I**) show the same analysis using flux measurements. The solid lines and shaded areas represent the mean value and standard derivations for each latitude region, respectively. Dotted regions indicated the partial correlations were significant at $p < 0.05$. A two-sided t test was used to assess the significance of the partial correlation analysis. Source data are provided as a Source Data file.

sensitivities, and even fewer CMIP6 models showed positive sensitivities. Additionally, we assessed the accuracy of these models in predicting the sign of the DFS-P_{freq} relationship at each pixel level, comparing these predictions with observations (Fig. 3C). About half of all pixels showed mismatches, highlighting the models' limited accuracy in capturing the DFS-P_{freq} correlations.

Discussion

Previous study has demonstrated the importance of P_{freq} on leaf onset timing in spring, supplementing the well-known dominant role of temperature on spring phenology[16]. However, the internal and external signals that trigger tree dormancy release remain unclear[23,24]. In this study, we reveal the effect of P_{freq} on autumn leaf senescence, a factor that has been largely overlooked. We find a positive correlation between DFS and P_{freq}. Accordingly, the widespread declines in the P_{freq} over the past four decades have led to earlier DFS in northern ecosystems. The impact of these changes varies among plant functional types, reflecting the diversity of strategies plants use to adapt to local environments and respond to climate change factors[25]. Limited soil moisture due to reduced P_{freq} can cause drought stress, negatively affecting soil organic carbon (SOC) levels and soil respiration[26,27]. Conversely, excessive moisture can also hinder respiration by reducing oxygen availability, which may explain observations of earlier DFS in regions with increased precipitation[28]. The interaction between soil moisture, heat, SOC, soil microorganisms, as well as soil geochemical characteristics defines the optimal conditions for plant growth[29,30].
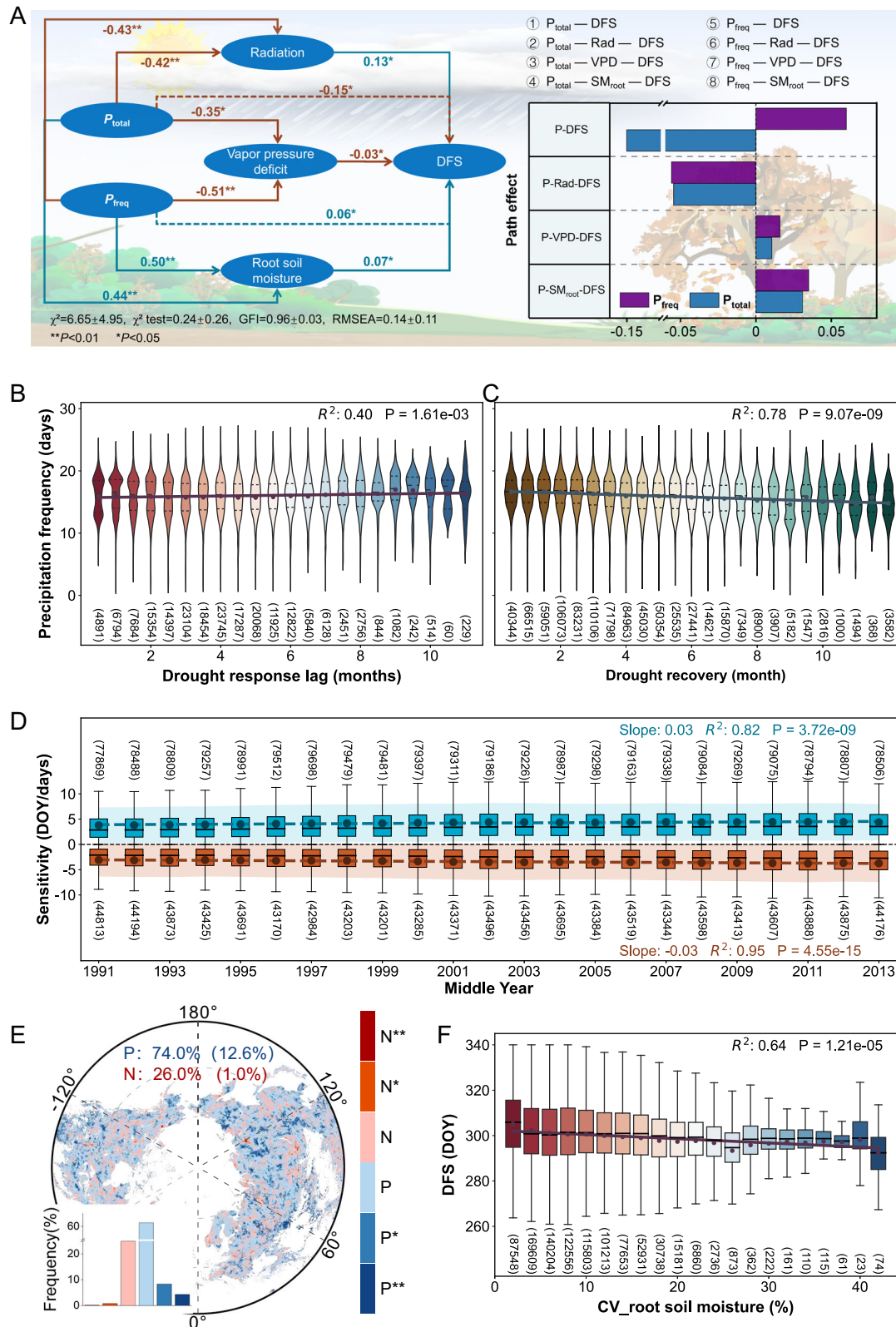
Fig. 2 | Mechanisms for the correlation between precipitation frequency and the dates of leaf senescence (DFS). Panel (**A**) shows the structural equation model (SEM) analysis. Panels (**B**, **C**) represent the changes of drought response lag and drought recovery time with precipitation frequency. Panel (**D**) shows the moving window approach with respect of positive and negative sensitivities of DFS to precipitation frequency over 1982–2022 (see "Methods"). Panel (**E**) shows the relationship between precipitation frequency and the maximum daily precipitation size (N and P represent negative and positive correlations). Panel (**F**) represents the correlation between DFS and root zone soil moisture variability using coefficients of variation (%). Box plots display means (solid dots), medians (horizontal lines), the 25th and 75th percentiles (box edges), and minimum and maximum values (whiskers). The shaded background represents the standard deviation. The numbers in parentheses represent the number of pixels in the corresponding region. * and ** represent $p < 0.05$ and $p < 0.01$, respectively. The significance level was evaluated using a two-sided t test. Source data are provided as a Source Data file.
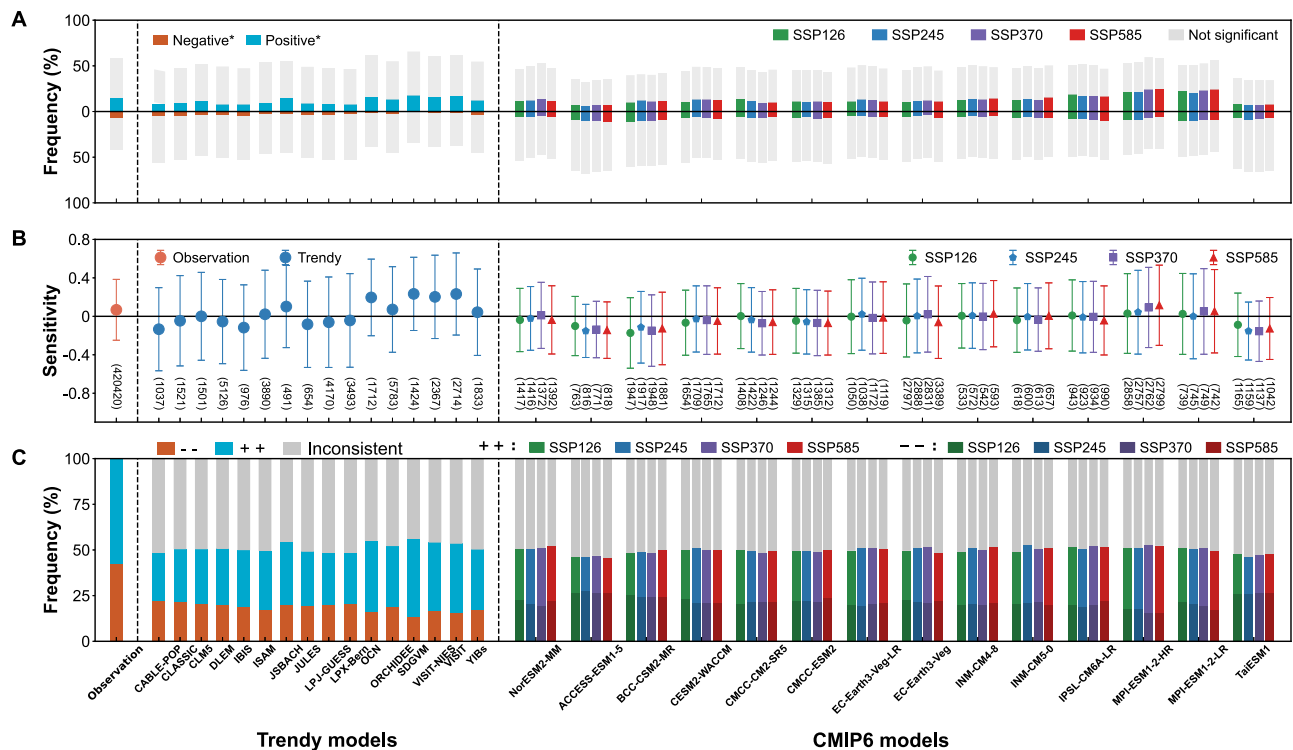
Fig. 3 | The test of Earth system models in reproducing the observed relationship between the dates of leaf senescence (DFS) and precipitation frequency. Panel (**A**) shows the overall proportions of significant positive and negative correlations. Panel (**B**) represents the sensitivity of DFS to precipitation frequency changes. Panel (**C**) is the comparison on the signs of correlation for each pixel. Four shared socioeconomic pathways (SSPs) were included for CMIP6 models, including SSP126, SSP245, SSP370, and SSP585, respectively. The solid symbols represent mean values and error bars indicate standard derivations. The numbers in parentheses indicate the number of pixels in the observation and each model. -- and ++ represent consistent negative and positive observations. Significance was set with $p < 0.05$ (two-sided t test). Source data are provided as a Source Data file.

These conditions are the result of long-term adaptation strategies developed by plants. Changes in P_{freq} alter these soil properties and this may prompt plants to adjust their DFS to enhance survival in changing environments. This adjustment may also reflect the increased demand for soil resources, particularly soil moisture, to sustain photosynthetic activity in a warming climate. Overall, our findings underscore the importance of considering seasonal precipitation patterns, rather than just total amounts, in understanding leaf senescence timing. This insight is crucial for incorporating temporal changes in precipitation into future ecosystem models to better understand the impacts of climate change on plant phenology and growth.

In our study, we aimed to elucidate the mechanisms behind the observed trend of earlier DFS with decreased P_{freq}, a task complicated by the interactive effects of precipitation amount and variability on terrestrial ecosystem processes[31]. Using partial correlation and SEM techniques, we identified that the earlier DFS under reduced P_{freq} is likely associated with intensified water constraints on photosynthesis, potentially driven by significant reductions in root-zone moisture and increases in VPD. A lower frequency of rainfall events implies longer drought periods. Consequently, soil moisture gradually declines, particularly in the surface layers where the majority of a plant's roots are concentrated. This poses a challenge for plants to access adequate water supply, especially after prolonged drought periods. Experimental studies have indicated that plant photosynthesis and primary productivity are significantly impacted by changes in P_{freq}[15]. Reduced P_{freq}, often coupled with smaller precipitation events, adversely affects soil moisture recharge and increases soil moisture variability, which potentially contributes earlier leaf senescence. The increase in atmospheric dryness further accelerates the cessation of photosynthesis.

Our results showed that there could be a trade-off effect on DFS between precipitation frequency and the total precipitation, by affecting radiation and soil moisture. In particular, the most important finding is that the significant decreasing trend of precipitation frequency, and its impact on the interannual variability of DFS trend. These results could be useful for the prediction of future ecosystem functions in responding to climate change by including the frequency of precipitation, rather the total for its unclear trends globally. In addition, the earlier DFS with declining P_{freq} may be explained by the "sink limitation" effect[6]. Our study demonstrates that a widespread decline in P_{freq} leads to soil moisture shortages, which, in turn, reduces the growth capacity related to water availability and ultimately results in earlier DFS. This "sink limitation" effect is indirectly supported by the finding of earlier DFS associated with a larger CV in soil moisture, as large changes in soil moisture CV indicate a harsher environment for plant growth[15].

A pivotal finding of our research is the identification of a significantly shortened drought response lag associated with decreased P_{freq}, a process representing drought acclimation. In particular, we found a significant negative correlation between drought response lag and evapotranspiration (ET) (Supplementary Fig. 7A). Such results imply an enhanced water-use strategy of plants that further supports plant adaptation and acclimation, probably by strengthening the growth of root systems to extend downstream for deeper water sources under droughts[32]. This reason has been supported by our results showing increased root depth with lower drought response lag (Supplementary Fig. 7 B). The enhanced drought acclimation is likely linked to the adaptive strategy of plants that have been exposed to prolonged periods of drought, including more effective water management and utilization. Plants can rapidly reduce water loss or increase water uptake when water availability is scarce through

morphologically deeper roots and an enhanced tolerance to drought physiologically by accumulating osmoprotectants and other regulatory substances[33]. Our observations, encompassing a wide range of species with varied plant functional types and local climatic backgrounds, therefore confirm and extend the critical role of P_{freq} on vegetation growth beyond site-level experiments.

We show that while current Earth system models were able to reproduce the overall trend in the correlation between DFS and P_{freq}, they inaccurately represent the sensitivity of DFS to changes in P_{freq}. A pixel-by-pixel analysis showed that these models incorrectly predict the sign of the DFS- P_{freq} correlation for half of the regions examined. This discrepancy may be primarily due to the models' reliance on the link between total precipitation and soil moisture, overlooking the significant effects of P_{freq} on ecosystem functions. However, the timing, frequency and duration of precipitation events are determinants of ecosystem processes during autumn[20,34,35] and therefore important for leaf senescence, as shown by our observations. Therefore, current Earth system models, driven by basic conceptual frameworks that ignore the effects of P_{freq} on plant hydraulics, fall short in reproducing the temporal effects of P_{freq} on DFS[36]. Including P_{freq} —a key measure of precipitation variability—into ecosystem models therefore has large potential to improve future predictions of drought impacts on ecosystems, especially given the expectation that future droughts will intensify in several dimensions, including magnitude, duration, timing, and frequency[11,37].

Methods

Study area
The Northern Hemisphere represents a particularly compelling focus for this study due to its vast and diverse biomes, which range from boreal forests to temperate woodlands and grasslands. This region contains a significant proportion of the world's terrestrial vegetation and carbon stocks, making it a critical area for studying phenological responses to climate variability. Additionally, the Northern Hemisphere is where some of the most pronounced climate changes, including alterations in precipitation patterns, have been observed in recent decades[38]. Monitoring the dynamics of vegetation in the Northern Hemisphere is crucial for understanding and mitigating climate. In this study, we focused on middle and high latitude regions of Northern Hemisphere (>30°N), where vegetation dynamic has an evident seasonality. We divided the study area into seven plant functional types according to the biome classification from the terrestrial ecoregions map[39], including temperate broadleaf forests (TBF), temperate coniferous forests (TCF), boreal forests (BF), temperature grasslands (TG), montane grasslands (MG), tundra (TD), and xeric shrublands (XS) (Supplementary Fig. 1).

Site-level DFS from flux data
The site-level phenology observations were derived from daily gross primary productivity (GPP) based on the eddy-covariance flux measurements. We removed sites with insufficient observations (<8 yr). As a result, 52 flux sites with a total of 662 year-site records of daily GPP from the FLUXNET database were selected (Supplementary Data 2). The use of GPP to extract phenological stages is a valid approach for observing vegetation phenology, as changes in GPP throughout the year can effectively indicate key phenological events. In this study, we used the end of growing season, derived from GPP time series, to represent the DFS observed at ground level. To obtain smoothed daily GPP curves, we employed a negative exponential approach that utilizes polynomial regression, where weights were assigned based on a Gaussian density function. This method effectively reduces noise in the GPP time series, providing a more accurate representation of the seasonal variations in photosynthetic activity. Subsequently, we defined DFS as the date when daily GPP declined to 10% of the annual maximum GPP[40] (Supplementary Fig. 8A).

Satellite derived DFS
The long time series of continuous NDVI dataset from the GIMMS-3G+ product was used to derive large-scale DFS across the Northern Hemisphere (>30°N). This dataset was based on corrected and calibrated measurements from Advanced Very High Resolution Radiometer (AVHRR) data[41] with a spatial resolution of 0.0833 degree and a half-month interval for 1982 to 2022.

To better capture the seasonal signals of vegetation while eliminating the interference of atmospheric effects and snow cover, the NDVI time series was fist reconstructed by weighted Whittaker algorithm[42]. Then a seven-parameter double logistic function[43] was used to fit the NDVI time series and DFS was determined based on inflection method[44].

$$f(t) = m_1 + (m_2 - m_7 \cdot t) \left(\frac{1}{1 + e^{(m_3 - t)/m_4}} - \frac{1}{1 + e^{(m_5 - t)/m_6}} \right) \quad (1)$$

where, m_1 is background NDVI; m_2 is the difference between summertime NDVI and background value; m_3 and m_5 are the midpoints in the days of the year of the transitions of spring green-up and autumn senescence, respectively; m_4 and m_6 are normalized slope coefficients for these transitions; m_7 is summer green-down parameter. DFS was defined as the time when the curvature changing rate reached its last local maximum value (Supplementary Fig. 8 B).

Simulated DFS from Trendy and CMIP6
We simulated DFS based on output GPP from 16 Trendy models during 1983–2021 (Supplementary Data 3) and 14 CMIP6 models under different shared socioeconomic pathways (SSPs) during 2016–2100 (Supplementary Data 4). SSPs refer to a set of standardized scenarios developed to facilitate the analysis of climate impacts, adaptation, and mitigation. These pathways describe different trajectories for future global development based on varying assumptions about population growth, economic development, technological advancements, and policy decisions[45]. For each CMIP6 model, we used the modeled GPP data from four SSPs (SSP-126, SSP-245, SSP-370, and SSP-585) to represent scenarios with low, moderate, high, and very high challenges to mitigation and adaptation, respectively. GPP is closely related to key factors like vegetation coverage, leaf area index, temperature and precipitation, which are crucial in shaping vegetation phenology. Consequently, the annual variation in GPP effectively reflects the phenological stages of vegetation. Based on this theoretical foundation, we first applied cubic spline interpolation to improve data continuity, given that most GPP datasets are available at a monthly temporal resolution. We then fitted the GPP time series using the seven-parameter double logistic function (Eq. 1), defining DFS as the date when the rate of curvature change reached its last local maximum value (Supplementary Fig. 8C).

Climate data
We derived monthly total amount (P_{total}) and frequency (P_{freq}) of precipitation from two independent datasets: (1) the Climatic Research Unit Time-Series (CRU TS 4.07) and (2) the fifth generation European Center for Medium-Range Weather Forecasts reanalysis of the global climate (ERA5). The CRU dataset is produced by the interpolation from extensive networks of climatic station observations and provides several climate variables on a 0.5° × 0.5° spatial resolution and a monthly temporal resolution[46]. We used wet day frequency, which defined as days with ≥0.1 mm precipitation, as P_{freq}. The ERA5 product provides hourly estimates of various climate variables with a spatial resolution of 0.1° based on vast amounts of historical observations[47]. We obtained total precipitation from the monthly aggregated datasets and calculated the number of rainy days per month based on the daily precipitation (≥0.1 mm). We used the mean value of P_{total} and P_{freq}

from CRU and ERA5 as final P_{freq} and P_{total} for 1982–2022 to reduce the uncertainty from a single dataset. Monthly mean temperature was obtained from CRU and surface net solar radiation was accessed from ERA5. Vapor pressure deficit (VPD) and evapotranspiration (ET) data for 1982–2022 were obtained from TerraClimate with a monthly temporal resolution and a 1/24 degree spatial resolution. The monthly root-zone soil moisture from 1982 to 2022 was obtained from Global Land Evaporation Amsterdam Model (GLEAM) with a spatial resolution of 0.25°.

Identification of drought events, drought recovery and drought response lag

Extreme drought events were identified by examining monthly SPEI-3 (Standardized Precipitation-Evapotranspiration Index at a 3-month scale) values below the threshold of -2. Drought recovery is defined as the duration (months) starting from the month with the deepest suppression of NDVI to the month when NDVI returns to within 95% of the long-term average baseline in each pixel. The monthly SPEI3 and NDVI time series were first smoothed by a 3-month forward moving window, they were then sequentially deseasonalized and linearly detrended. To avoid lengthening the drought recovery duration due to algorithm design, if vegetation recovery extending through the dormant season and into subsequent year, the drought recovery was calculated as the total length of the recovery period minus the length of the dormant season. We measured response lag in months, which is the time between the lowest SPEI3 value and the most significant drop in NDVI caused by drought. We calculated both drought response lag and recovery time for each pixel individually.

Analysis

Precipitation, along with temperature and radiation, collectively regulate DFS[48]. In addition, covariate effects exist among these climatic variables as well. Therefore, we applied partial correlation analysis to explore the impacts of P_{total} and P_{freq} on DFS. Given that the potential biases between flux-based and satellite-based measurements of DFS, we did not combine these two data in the subsequent analyses. Instead, we conducted separate analyses for each measure of DFS to ensure the validity of the results. In the analysis of satellite-based DFS, we used gridded climate data that were resampled using the bilinear interpolation method to match the spatial resolution of the satellite-based DFS. For the flux-based DFS, we directly extracted the corresponding climate data from these gridded datasets based on the coordinates of each flux site. We performed partial correlation analysis under three schemes: (1) partial correlation between DFS and P_{total}, removing the effects of temperature and radiation (scheme 1); (2) partial correlation between DFS and P_{total}, removing the effects of temperature, radiation, and P_{freq} (scheme 2); (3) partial correlation between DFS and P_{freq}, removing the effects of temperature, radiation, and P_{total} (scheme 3). Preseason forcings have a better predictive strength on phenology than fixed seasonal climate forcing alone[4,49]. We thus used the preseason mean values of each climatic variable in the partial correlation analysis. For example, the preseason length of P_{freq} was defined as the period when the absolute value of partial correlation coefficient between P_{freq} and DFS was at its maximum. For each pixel, the preseason periods of 0 to 6 months prior to the multi-year mean DFS were examined (Supplementary Fig. 9).

To investigate the temporal changes in the sensitivity of DFS to P_{freq}, we used a moving window method. We conducted tests on a variety of window sizes, ranging from 10 to 20 years. For each window size, we calculated the sensitivity of DFS to P_{freq} based on multilinear regression within each moving window. Then we calculated the percentages of significant sensitivity ($P < 0.05$) and fitted these values to obtain the optimal window size with the largest R^2. As a result, the optimal window size was set as 19 years to perform subsequent analyses (Supplementary Fig. 10).

$$DFS = a \cdot P_{freq} + b \cdot P_{total} + c \cdot \text{Temperature} + d \cdot \text{Radiation} + \varepsilon \quad (2)$$

where, a, b, c and d are regression coefficients and represent the sensitivity of DFS to P_{freq}, P_{total}, temperature, and radiation, respectively. ε is the residual error. All the climate variables used in the regression were the mean values during preseason.

To explore the potential mechanisms by which precipitation affects DFS, we performed structural equation modeling (SEM), a statistical technique used to test and estimate causal relationships using both direct and indirect paths. We hypothesized that the effect of precipitation patterns on DFS is mediated by their impact on solar radiation and drought conditions. To test this hypothesis, we constructed an SEM that included three mediating variables: radiation, VPD, which indicates atmospheric dryness, and root-zone soil moisture. Path coefficients were estimated using maximum likelihood estimation. Additionally, we assessed the model's applicability and effectiveness by calculating various statistics and fit indices, such as the chi-square test, the goodness-of-fit index (GFI), and the root mean square error of approximation (RMSEA). The SEM was initially applied to each pixel across the entire study area, and we subsequently selected pixels with a significance level of $p < 0.05$. The mean values of their corresponding coefficients were calculated to determine the final path coefficients.

Reporting summary

Further information on research design is available in the Nature Portfolio Reporting Summary linked to this article.

Data availability

All data used in this study can be obtained from open-access databases. The NDVI data is from Global Inventory Modeling and Mapping Studies-3rd Generation V1.2 (GIMMS-3G +) and can be accessed from https://daac.ornl.gov/cgi-bin/dsviewer.pl?ds_id=2187. The ERA5 data can be accessed from https://cds.climate.copernicus.eu/cdsapp#!/dataset/reanalysis-era5-land-monthly-means?tab=overview. The CRU data can be accessed from https://crudata.uea.ac.uk/cru/data//hrg/. The TerraClimate data can be accessed from https://climate.northwestknowledge.net/TERRACLIMATE/index_animations.php/. The Root-Zone Soil Moisture data can be accessed from https://www.gleam.eu/. The root depth data can be accessed from https://wci.earth2observe.eu/thredds/catalog/usc/root-depth/catalog.html. Source data are provided with this paper. The complete and derived data are also stored in a publicly available Zenodo repository (https://doi.org/10.5281/zenodo.14359346). Source data are provided with this paper.

Code availability

All data analyses and modeling were performed using MATLAB R2023b and R 4.3.1. The code is stored in a publicly available Zenodo repository (https://doi.org/10.5281/zenodo.14359346).

References

1. Peaucelle, M., Peñuelas, J. & Verbeeck, H. Accurate phenology analyses require bud traits and energy budgets. *Nat. Plants* **8**, 915–922 (2022).
2. Li, Y. et al. Widespread spring phenology effects on drought recovery of Northern Hemisphere ecosystems. *Nat. Clim. Chang.* **13**, 182–188 (2023).
3. Shen, M. et al. Plant phenology changes and drivers on the Qinghai–Tibetan Plateau. *Nat. Rev. Earth Environ.* **3**, 633–651 (2022).
4. Piao, S. L. et al. Leaf onset in the northern hemisphere triggered by daytime temperature. *Nat. Commun.* **6**, 6911 (2015).

5. Stuble, K. L., Bennion, L. D. & Kuebbing, S. E. Plant phenological responses to experimental warming—A synthesis. *Glob. Change Biol.* **27**, 4110–4124 (2021).

6. Zani, D., Crowther, T. W., Mo, L., Renner, S. S. & Zohner, C. M. Increased growing-season productivity drives earlier autumn leaf senescence in temperate trees. *Science* **370**, 1066–1071 (2020).

7. Chen, L. et al. Leaf senescence exhibits stronger climatic responses during warm than during cold autumns. *Nat. Clim. Chang.* **10**, 777–780 (2020).

8. Zohner, C. M. et al. Effect of climate warming on the timing of autumn leaf senescence reverses after the summer solstice. *Science* **381**, 6653 (2023).

9. Xu, C. G. et al. Increasing impacts of extreme droughts on vegetation productivity under climate change. *Nat. Clim. Chang.* **9**, 948–953 (2019).

10. Peñuelas, J. et al. Complex spatiotemporal phenological shifts as a response to rainfall changes. *N. Phytol.* **161**, 837–846 (2004).

11. Knapp, A. K. et al. Field experiments have enhanced our understanding of drought impacts on terrestrial ecosystems—But where do we go from here? *Funct. Ecol.* **38**, 76–97 (2024).

12. Zhang, Y., Parazoo, N. C., Williams, A. P., Zhou, S. & Gentine, P. Large and projected strengthening moisture limitation on end-of-season photosynthesis. *Proc. Natl Acad. Sci. Usa.* **117**, 9216–9222 (2020).

13. Kannenberg, S. A. et al. Dominant role of soil moisture in mediating carbon and water fluxes in dryland ecosystems. *Nat. Geosci.* **17**, 38–43 (2024).

14. Wu, C. et al. Increased drought effects on the phenology of autumn leaf senescence. *Nat. Clim. Chang.* **12**, 943–949 (2022).

15. Knapp, A. K. et al. Rainfall variability, carbon cycling, and plant species diversity in a mesic grassland. *Science* **298**, 2202–2205 (2002).

16. Wang, J. et al. Decreasing rainfall frequency contributes to earlier leaf onset in northern ecosystems. *Nat. Clim. Chang.* **12**, 386–392 (2022).

17. Feldman, A. F. et al. Plant responses to changing rainfall frequency and intensity. *Nat. Rev. Earth Environ.* **5**, 276–294 (2024).

18. Zhang, Z. Z. et al. Prolonged dry periods between rainfall events shorten the growth period of the resurrection plant Reaumuria soongorica. *Ecol. Evol.* **8**, 920–927 (2018).

19. Post, A. K. & Knapp, A. K. The importance of extreme rainfall events and their timing in a semi-arid grassland. *J. Ecol.* **108**, 2431–2443 (2020).

20. Jin, H. et al. Higher vegetation sensitivity to meteorological drought in autumn than spring across European biomes. *Commun. Earth Environ.* **4**, 299 (2023).

21. Piao, S. et al. Plant phenology and global climate change: Current progresses and challenges. *Glob. Change Biol.* **25**, 1922–1940 (2019).

22. Zhang, Y. et al. Increasing sensitivity of dryland vegetation greenness to precipitation due to rising atmospheric CO_2. *Nat. Commun.* **13**, 4875 (2022).

23. Singh, R. K. et al. Photoperiod- and temperature-mediated control of phenology in trees – a molecular perspective. *N. Phytol.* **213**, 511–524 (2017).

24. Yumoto, G. et al. Seasonal switching of integrated leaf senescence controls in an evergreen perennial Arabidopsis. *Nat. Commun.* **15**, 4719 (2024).

25. Seddon, A. et al. Sensitivity of global terrestrial ecosystems to climate variability. *Nature* **531**, 229–232 (2016).

26. Jackson, R. B. et al. The ecology of soil carbon: pools, vulnerabilities, and biotic and abiotic controls. *Annu. Rev. Ecol. Evol. Syst.* **48**, 419–445 (2017).

27. Huang, N. et al. Spatial and temporal variations in global soil respiration and their relationships with climate and land cover. *Sci. Adv.* **6**, eabb8508 (2020).

28. Buitenwerf, R., Rose, L. & Higgins, S. Three decades of multi-dimensional change in global leaf phenology. *Nat. Clim. Change* **5**, 364–368 (2015).

29. Knapp, A. K., Ciais, P. & Smith, M. D. Reconciling inconsistencies in precipitation-productivity relationships: Implications for climate change. *N. Phytologist* **214**, 41–47 (2017).

30. Fu, Z. et al. Atmospheric dryness reduces photosynthesis along a large range of soil water deficits. *Nat. Commun.* **13**, 989 (2022).

31. Felton, A. J. et al. Precipitation amount and event size interact to reduce ecosystem functioning during dry years in a mesic grassland. *Glo. Chan. Bio.* **26**, 658–668 (2020).

32. Li, D. et al. Declining coupling between vegetation and drought over the past three decades. *Glo. Chan. Bio.* **30**, e17141 (2024).

33. Zhou, H. et al. Climate warming interacts with other global change drivers to influence plant phenology: A meta-analysis of experimental studies. *Ecol. Lett.* **26**, 1370–1381 (2023).

34. Komatsu, K. J. et al. Global change effects on plant communities are magnified by time and the number of global change factors imposed. *Proc. Natl Acad. Sci. Usa.* **116**, 17867–17873 (2019).

35. Jiao, W. et al. Observed increasing water constraint on vegetation growth over the last three decades. *Nat. Commun.* **12**, 3777 (2021).

36. Paschalis, A. et al. Rainfall manipulation experiments as simulated by terrestrial biosphere models: Where do we stand? *Glo. Chang. Biolo.* **26**, 3336–3355 (2020).

37. Donat, M. et al. More extreme precipitation in the world's dry and wet regions. *Nat. Clim. Change* **6**, 508–513 (2016).

38. Gulev, S. K. et al. Changing State of the Climate System. In Climate Change 2021: The Physical Science Basis. Contribution of Working Group I to the Sixth Assessment Report of the Intergovernmental Panel on Climate Change. Cambridge University Press, 287–422. https://doi.org/10.1017/9781009157896.004.

39. Olson, D. M. et al. Terrestrial Ecoregions of the World: A New Map of Life on Earth: A new global map of terrestrial ecoregions provides an innovative tool for conserving biodiversity. *BioScience* **51**, 933–938 (2001).

40. Wu, C. Y. et al. Interannual variability of net ecosystem productivity in forests is explained by carbon flux phenology in autumn. *Glob. Ecol. Biogeogr.* **22**, 994–1006 (2013).

41. Pinzon, J. & Tucker, C. A Non-Stationary 1981–2012 AVHRR NDVI3g Time Series. *Remote Sens.* **6**, 6929–6960 (2014).

42. Kong, D. et al. A robust method for reconstructing global MODIS EVI time series on the Google Earth Engine. *Isprs J. Photogramm. Remote Sens.* **155**, 13–24 (2019).

43. Elmore, A. J. et al. Landscape controls on the timing of spring, autumn, and growing season length in mid-Atlantic forests. *Glob. Change Biol.* **18**, 656–674 (2012).

44. Zhang, X. et al. Monitoring vegetation phenology using MODIS. *Remote Sens. Environ.* **84**, 471–475 (2003).

45. O'Neill, B. C. et al. The roads ahead: Narratives for shared socio-economic pathways describing world futures in the 21st century. *Glob. Environ. Change* **42**, 169–180 (2017).

46. Harris, I. et al. Version 4 of the CRU TS monthly high-resolution gridded multivariate climate dataset. *Sci. Data* **7**, 109 (2020).

47. Hersbach, H. et al. The ERA5 global reanalysis. *Q. J. R. Meteorol. Soc.* **146**, 1999–2049 (2020).

48. Liu, Q. et al. Delayed autumn phenology in the Northern Hemisphere is related to change in both climate and spring phenology. *Glob. Change Biol.* **22**, 3702–3711 (2016).

49. Wu, C. et al. Contrasting responses of autumn-leaf senescence to daytime and night-time warming. *Nat. Clim. Change* **8**, 1092–1096 (2018).

Author contributions

C.W. designed the research. C.W., Xiaoyue W., and D.P. wrote the first draft of the manuscript. X.Z., Xiaoyue W., and P.S. performed the data analysis. C.M.Z., J.P., Y.L., Xiuchen W., Y.Z., H.L., X.J., W.L., D.T., P.P., and A.B.F. assessed the research analyses and contributed to the writing of the manuscript.

Competing interests

The authors declare no competing interests.

Additional information

Supplementary information The online version contains supplementary material available at https://doi.org/10.1038/s41467-025-56159-4.

Correspondence and requests for materials should be addressed to Xiaoyue Wang, Dailiang Peng or Chaoyang Wu.

Peer review information *Nature Communications* thanks Hongxiao Jin and the other, anonymous, reviewer(s) for their contribution to the peer review of this work. A peer review file is available.

Reprints and permissions information is available at http://www.nature.com/reprints

Publisher's note Springer Nature remains neutral with regard to jurisdictional claims in published maps and institutional affiliations.

[1]The Key Laboratory of Land Surface Pattern and Simulation, Institute of Geographic Sciences and Natural Resources Research, Chinese Academy of Sciences, 100101 Beijing, China. [2]University of the Chinese Academy of Sciences, 100049 Beijing, China. [3]Institute of Surface-Earth System Science, School of Earth System Science, Tianjin University, Tianjin 300072, China. [4]Department of Environmental Systems Science, Institute of Integrative Biology, ETH Zurich, Zurich, Switzerland. [5]CSIC, Global Ecology Unit CREAF-CSIC-UAB, Bellaterra, Barcelona 08193 Catalonia, Spain. [6]CREAF, Cerdanyola del Valles, Barcelona 08193 Catalonia, Spain. [7]School of Natural Resources and the Environment, University of Arizona, Tucson, AZ, USA. [8]State Key Laboratory of Earth Surface Processes and Resource Ecology, Faculty of Geographical Science, Beijing Normal University, Beijing, China. [9]Sino-French Institute for Earth System Science, College of Urban and Environmental Sciences, and Laboratory for Earth Surface Processes, Peking University, Beijing 100871, China. [10]Institute of Eco-Chongming (IEC), East China Normal University, Shanghai, China. [11]Integrated Research on Energy, Environment, and Society (IREES), Energy and Sustainability Research Institute Groningen (ESRIG), University of Groningen, Groningen, The Netherlands. [12]Potsdam Institute for Climate Impact Research (PIK), Member of the Leibniz Association, Potsdam 14473, Germany. [13]Unité de Recherche en Foresterie et Conservation des Bioressources, Ecole de Foresterie Tropicale, Université Nationale d'Agriculture, BP 43 Kétou, Benin. [14]Key Laboratory of Digital Earth Science, Aerospace Information Research Institute, Chinese Academy of Sciences, 100094 Beijing, China. ✉e-mail: wangxy@igsnrr.ac.cn; pengdl@aircas.ac.cn; wucy@igsnrr.ac.cn